Snap Buckling of a Constrained Photomechanical Switch Driven by Elastic Instability

Matthew L. Smith[*1], Andrew A. Sicard[1], Amir Alipour Skandani[2] and M. Ravi Shankar[2]
[1]Hope College, Department of Engineering, Holland, MI, USA, [2]University of Pittsburgh, Department of Industrial Engineering, Pittsburgh, PA, USA
*Corresponding author: 27 Graves Place, Holland, MI 49423, msmith@hope.edu

Abstract: Photomechanical materials convert light energy to mechanical work. This class of materials represents a unique opportunity for wireless actuation and morphing surface technology. Challenges for realizing functional devices with these materials include: producing controlled complex motion, low power output, and degradation in actuator behavior with use. A typical strategy for producing complex motion is to engineer materials with various material anisotropies. Recently we reported on a strategy for producing fast actuation rates (~10ms) and controlling positioning based in part on mechanical design concepts using snap-through of a photomechanical, buckled arch. Herein we, propose that rational use of geometric contact points will lead to enhanced, controllable complex motion for a multi-position, wireless actuator.

Keywords: *Light Responsive Materials, Elastic Instability, Actuators, Azobenzene, Polymers.*

1. Introduction

Photomechanical materials experience strains in response to light of various wavelengths. These remotely triggered, photo-induced strains lead to large-scale deformations, presenting significant opportunities for wireless actuators and light-driven morphing structures (Fig. 1a). A large space of possible mechanical behaviors exist for these materials since their response depends on a variety of system parameters such as the wavelength and polarization of light, material anisotropies and patterning, molecular morphology, etc. A particular area of focus in the literature is the control of three dimensional motion through patterned material anisotropies [1,2]. However, sample geometry, boundary conditions, and contact conditions are also extremely important, and rational mechanical design can add significantly to the response complexity and utility. Accurate simulations that address both material responses and coupled nonlinear structural responses are needed in order to streamline experimental efforts as well as for predicting system performance for useful work in functional devices.

Previously we investigated the snap-through of bistable arches triggered by light [3]. Bistable arches have the advantage that once they are in one of the two equilibrium configurations they can hold their position without the use of additional power. These arches display a slow build-up of elastic strain energy to a point of instability, and then they rapidly release this energy resulting in a fast actuation step (~10ms) between the two equilibrium states. The pattern of discrete functional behavior inherent in bistable actuators is valuable for applications such as binary robotics [4] and morphing surface topologies for applications like soft haptic displays. In this work we explore the design and implementation of contact conditions to enhance and extend the behavior of bistable arches into multistable structures that operate on the principle of light induced elastic instabilities.

Based on preliminary experimental results, we examine a photomechanical device (Fig. 1b) in which an elastic strip of light responsive material is buckled into contact with a rigid pin. Selective light irradiation leads to an elastic instability and eventual rapid snap buckling into a second stable configuration. We present a design that features same-sided snap-buckling. This particular design may prove useful in applications where limited space toggling or mechanical logic gates (not-gates) are required. We also show that this same device can also snap-through to a third stable position. This study lays a foundation for designing light triggered actuators in which contact and boundary conditions play a crucial role in enhancing the complexity of generated motion.

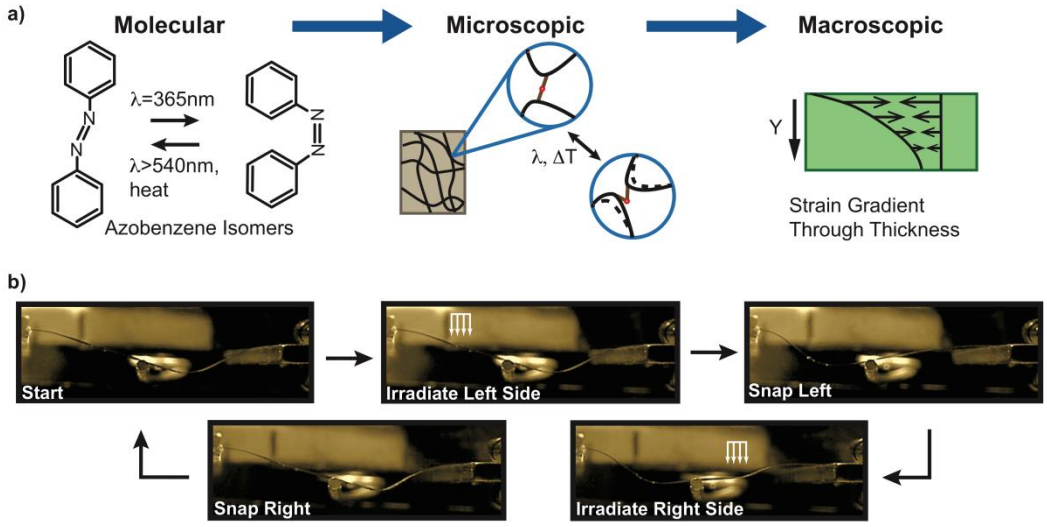

Figure 1. Azobenzene functionalized polyimides can convert light energy into mechanical work. a) Azobenzene is a molecule that can take on one of two shapes: the elongated *trans* isomer or the bent *cis* isomer. If these molecules are incorporated into a polymer network and a large enough population is activated at one time, then cooperative microscopic deformation leads to macroscopic deformations in thin structures. As the azobenzenes near the irradiated surface absorb the light there is less light to trigger isomerization deeper within the material. The result of this light attenuation is a strain gradient through the material thickness. b) A strip of azobenzene functionalized polyimide is buckled into a pin and then irradiated with uv (or in some cases blue-green) light. The light is polarized in the long direction of the strip, and focused on the left side to induce snap-buckling to the left. Snap-buckling back to the right can then be induced by irradiating the right side of the strip. The strip is approximately 40mm long, 1mm wide, and 15μm thick.

2. Methods

In this study we model the structure (Fig. 2) as a two dimensional, linear elastic solid. Simulations were performed using the structural mechanics module of COMSOL Multiphysics. Coordinates of material points in the reference configuration are given by $X \in [0, L_o]$ and $Y \in [-a/2\,, a/2]$. Displacements of material points are given by the vector $\boldsymbol{u}(X, Y, t)$. The standard implementation in COMSOL includes the equations of motion (1), constitutive equations (2), and the geometrically nonlinear strain-displacement relations (3),

$$\rho \frac{\partial^2 \boldsymbol{u}}{\partial t^2} = \nabla \cdot [\boldsymbol{S} \cdot \boldsymbol{F}^T], \qquad (1)$$

$$\boldsymbol{S} = \boldsymbol{C} : \varepsilon_{el}, \qquad (2)$$

$$\varepsilon = \frac{1}{2}[(\nabla \boldsymbol{u})^T + \nabla \boldsymbol{u} + (\nabla \boldsymbol{u})^T \nabla \boldsymbol{u}]\,, \qquad (3)$$

where ρ is the material density, $\boldsymbol{S}$ is the second Piola-Kirchhoff stress tensor, $\boldsymbol{F}$ is the deformation gradient, $\boldsymbol{C}$ is the stiffness tensor, and ε is the strain tensor. Material parameters that are entered into the the stiffness tensor using the COMSOL interface are Young's Modulus, E, and Poisson's ratio, ν. In all simulations the following values were used: $\rho = 1365$ kg/m^3, $E = 2.77$ GPa, and $\nu = 0.35$.

In this formulation $\varepsilon_{el} = \varepsilon - \varepsilon_{inel}$, where ε_{inel} is any inelastic contribution to the strain, such as from thermal expansion or in the case of the present work photo-induced strains. Since the light triggering motion is polarized parallel to the X direction the only photo-induced strains are,

$$\varepsilon_{inel\_X} = \varepsilon_X^{ph} = I(X)\beta e^{-(a/2-Y)/d}, \qquad (4)$$

$$\varepsilon_{inel\_\perp} = \varepsilon_\perp^{ph} = \nu^{ph} \varepsilon_X^{ph}, \qquad (5)$$

where $\varepsilon_\perp^{ph}$ are the induced strains in the direction perpendicular to the X direction due to a photo Poisson like effect with proportionality constant $\nu^{ph} = -0.3$. In equation (4), β is the proportionality constant between strain and intensity and is termed the photo compliance, $d = 7.7\mu$m is the attenuation length of the light, and $I(X)$ is the light intensity at the incident surface. Here we assume the intensity profile in

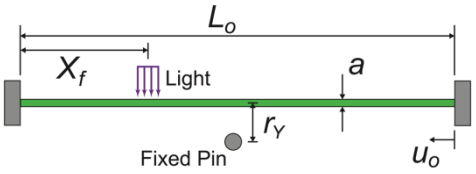

Figure 2. Schematic of the model reference configuration. X_f is the laser focus point and r_Y is the vertical position of the fixed pin as measured from the strip's centerline. In the simulations $L_o =$ 40 mm and for most of the simulations $a = 200\mu$m.

the X direction is approximated sufficiently by a boxcar function (cf. Fig. 2). The typical laser beam width in experiments is 5mm. The light induced, inelastic strain field is implemented using the initial strain subnode under the linear elastic materials node.

In a representative simulation, first, parameters such as the pin placement and laser focus point are set (see Fig. 2). Except for horizontal displacement at the right end, all displacements and rotations are restricted at the boundaries. Friction free contact surfaces are assigned between the bottom of the strip and the fixed pin. Then a time-dependent or stationary study is performed to compress the right end a specified amount, u_o, buckling the arch into the rigid pin. A slight load is applied at the beginning of this study to bias the buckling downward. For all simulations the horizontal position of the pin was set to $r_X/L_o = 0.4875$ as measured from the left end. As a result the arch slides over the pin and settles in a buckled position to the right. A second study (time-dependent) is performed in which the laser intensity is ramped up linearly until the arch reaches an elastic instability and rapidly snaps into a new position. The BDF solver with the automatic Newton method is used to perform these time-dependent studies.

3. Results and Discussion

Simulations were performed in order to identify qualitative relationships between key design

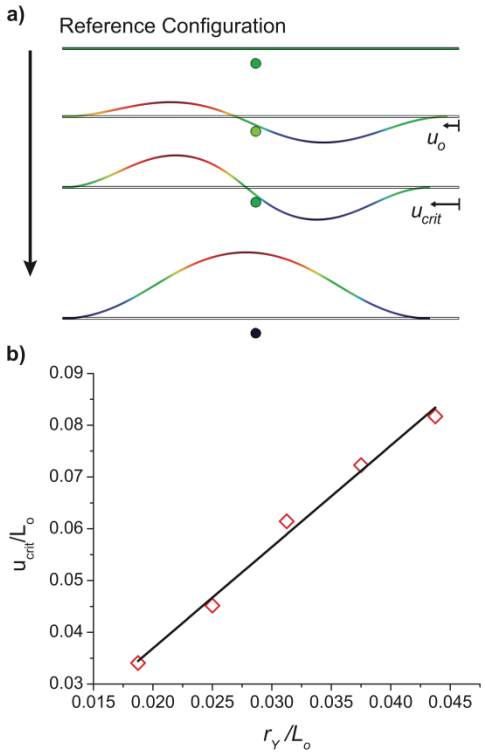

Figure 3. (a) Simulations of the arch buckling into the fixed pin as u_o is increased. At a critical displacement, u_{crit}, the structure becomes unstable and dynamically snaps upward. (b) The relationship between critical end displacement and the vertical pin position is represented well with a linear fit.

parameters and the overall behavior of the structure. The first series of simulations were performed without including irradiation effects. In these simulations u_o was increased until the arch became unstable and snapped into an upward buckled configuration (Fig. 3a). These simulations revealed a linear relationship between the vertical position of the pin and the critical end displacement (Fig. 3b). For the purpose of future simulations and experimental design, this data establishes limits for end displacements that are suitable for photo-induced snap as the pin position is varied vertically.

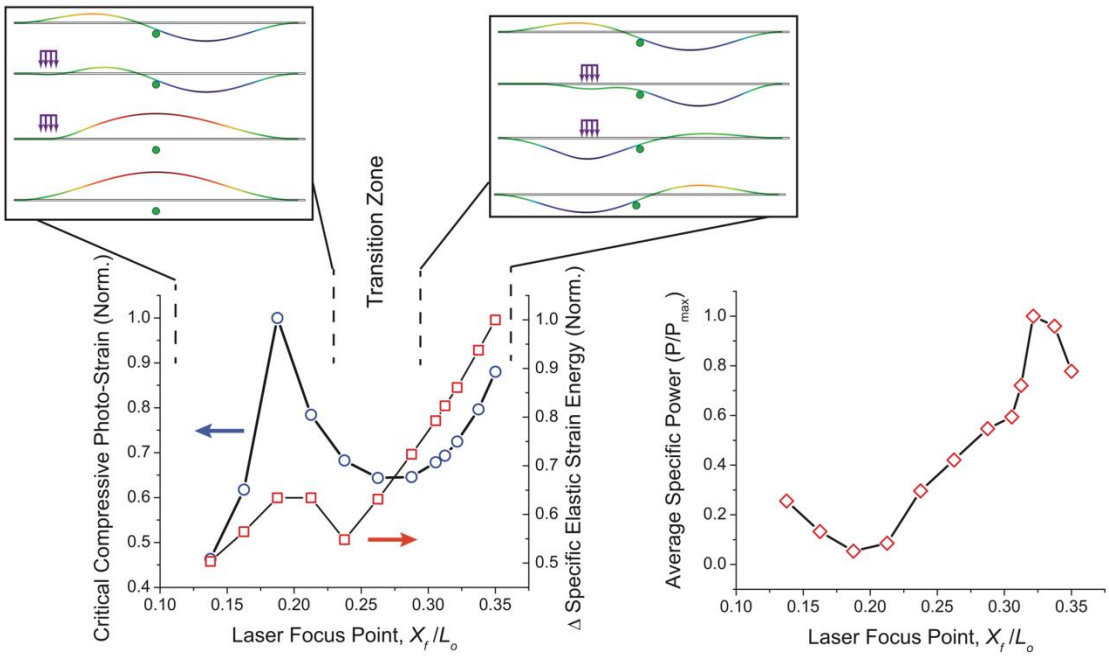

Figure 4. At left. Two different snap regimes are displayed: snap-up and snap-left. The normalized critical compressive photo-strain at the irradiated surface and specific strain energy difference are plotted as a function of laser focus point to compare the material behavior for these regimes. Each quantity was normalized by dividing by its maximum value over the entire range. At right. The average specific power is plotted as a function of laser focus point. In each simulation u_o/L_o was set to 0.9767 (nearly 1 mm for a 40 mm long strip).

A second series of simulations was performed to explore the effects of varying the location of the laser focus point (Fig. 4). Changes in the focus point of the laser reveal two response regimes, producing a discrete 3 position actuator: down left, down right, and up. In the initial buckled configuration, when the laser is focused moderately close to the pin the structure snaps to the left and down. For focus points very close to the pin the solver had difficulty converging. If so desired the structure can be snapped back to the right by irradiating the right side of the material strip (Fig 5). For focus points near the left boundary the structure always snaps to an upward configuration. In between the snap left and snap up regimes there seemed to be a transition zone in which the simulations were particularly sensitive to model inputs and both states could be obtained. In all cases there exists a small period of transient oscillations lasting typically less than 20 ms, but in some cases up to 200 ms.

For these simulations the critical compressive photo-strain at the irradiated surface was plotted as a function of laser focus point (Fig. 4). In addition the change in specific elastic strain energy between the point of instability and the newly attained equilibrium configuration (just after snap) was plotted. The overall trends show that the equilibrium energy difference between the two states increases when the laser is focused near the pin, but the required photo-strain is also relatively high in that region. In absolute terms, the simulations predict photo-strains on the order of 1-3%, which is more realistic for elastomeric materials, but is less expected for glassy polyimides. These strain levels also push beyond the anticipated limits of linear elasticity. This result is primarily due to the simulated material thickness of 200μm in comparison to the experimental thickness of 15 μm, where much smaller strains are required for the onset of elastic instability. Nonetheless, the qualitative trends revealed here still provide some insight into the behavior we can expect from this system.

From this same series the specific power was calculated by dividing the specific energy difference by the time required for the structure to evolve from the point of instability to the

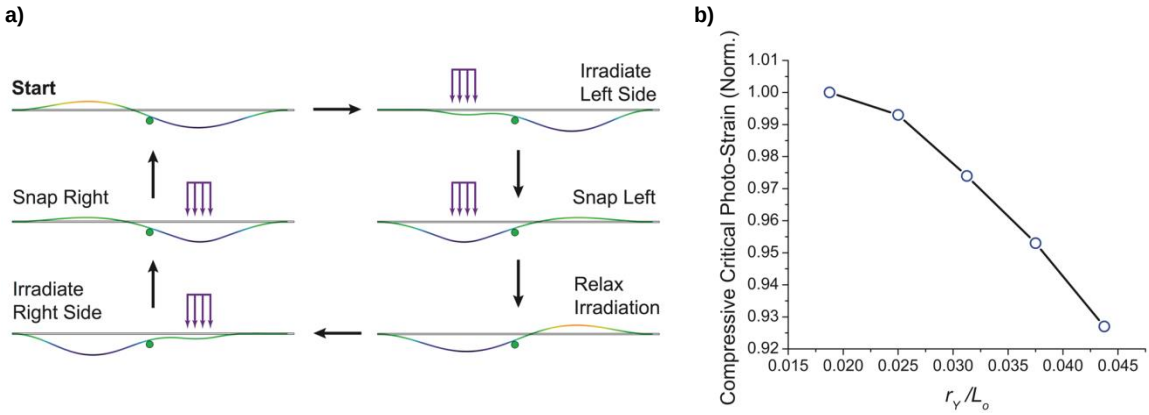

Figure 5. (a) In simulations the buckled structure can be cycled between the left and right snapped-down configurations by alternating the location of the laser focus point. In the experimental system some history is usually imparted by the irradiation. As a result, when the irradiation is removed the structure does not completely relax. Future models should also attempt to incorporate these effects. (b) The critical compressive photo-strain at the irradiated surface is shown as a function of the vertical pin position while all other parameters are held fixed.

snapped-left or up state. The time selected was just after the transient modes died off. Again higher specific powers were predicted for laser focus points near the pin. The max specific power predicted was on the order of that produced by flight muscles in some birds (~500 W/kg) [5] but below the instantaneous specific powers of the most powerful muscles and elastic energy release mechanisms in nature [6,7]. The instantaneous specific power density taken from the first transient oscillation was usually larger. However, due to the overly large induced strains it is likely these predicted powers are an overestimate. Further modeling using rubber elasticity or thinner structures should be performed to refine and extend these results.

The pin position is potentially one important design parameter affecting actuator performance. In this preliminary work, we investigated the effect of the vertical pin position on critical photo-strain (Fig. 5b). As the pin position decreases (moves closer to the reference configuration centerline) the critical photo-strain increases monotonically. However, the critical photo-strain appears to be only marginally sensitive to the vertical pin position, since over a fairly large range of positions (decrease of 60% from the maximum pin position) the critical photo-strain only changes by about 7.5%. Therefore, in the design of a functional actuator other factors besides critical light intensity (photo-strain) should be able to dominate the selection of the pin position.

4. Conclusions

Photomechanical materials offer exciting opportunities for versatile functional design from wireless actuators to light induced morphing surfaces. Though, often complex motion is designed into these materials using local anisotropies, here we have explored an alternate route to controlled, large configuration changes via additional geometric contact points. We have shown preliminary qualitative results concerning the effect of system parameters on critical photo-strains leading to snap-motion and specific power output. Perhaps more importantly we have shown that by using these contacts and careful placement of the triggering light we can produce a multistable actuator with three different stable positions. This result indicates that an additional pin could be placed opposite the current pin to potentially produce a discrete 4 position actuator. This additional functionality along with the potential to couple several actuators together substantially increases the options a designer has for producing intricate movements. Future studies will focus on improving the material model and systematically exploring the space of enhanced actuator designs based on arches with geometric contact.

5. Acknowledgements

The authors gratefully acknowledge funding from the Air Force Office of Scientific Research.

The computational work was performed at Hope College, while the experimental work was performed at the University of Pittsburgh.

6. References

1. Lee, K. M., Smith, M. L., et al. Photodriven, flexural-torsional oscillations of glassy azobenzene liquid crystal polymer networks, *Adv. Func. Mater.*, **21**, 2913-2918 (2011)
2. de Haan L. T., Sanchez-Somolinos, C. et al., Engineering of Complex Order and the Macroscopic Deformation of Liquid Crystal Polymer Networks, *Angew. Chem. Int. Ed.*, **51**, 12469-12472 (2012)
3. Shankar, M. R., Smith, M. L., et al. Contactless, photoinitiated snap-through in azobenzene-functionalized polymers, *PNAS*, **110**, 18792-18797 (2013)
4. Hafez, M. Lichter, M. D., and Dubowsky, S., Optimized Binary Modular Reconfigurable Robotic Devices, *IEEE/ASME Trans. on Mechatronics.*, **8**, 18-25 (2003)
5. Chai, P. and Millard, D., Flight and size constraints: Hovering performance of large hummingbirds under maximal loading, *J. Exp. Biol.*, **200**, 2757-2763 (1997)
6. Askew, G. N. and Marsh, R. L., The mechanical power output of the pectoralis muscle of blue-breasted quail (*Coturnix chinensis*): the *in vivo* length cycle and its implications for muscle performance, *J. Exp. Biol.*, **204**, 3587-3600 (2001)
7. Van Wassenbergh, S., Strother, J. A., et al. Extremely fast prey capture in pipefish is powered by elastic recoil, *J. R. Soc. Interface*, **5**, 285-296, (2008)